Multidimensional equilibria and their stability in copolymer-solvent mixtures

Karl Glasner [*], Saulo Orizaga [†]

Abstract

This paper discusses localized equilibria which arise in copolymer-solvent mixtures. A free boundary problem associated with the sharp-interface limit of a density functional model is used to identify both lamellar and concentric domain patterns composed of a finite number of layers. Stability of these morphologies is studied through explicit linearization of the free boundary evolution.

For the multilayered lamellar configuration, transverse instability is observed for sufficiently small dimensionless interfacial energies. Additionally, a crossover between small and large wavelength instabilities is observed depending on whether solvent-polymer or monomer-monomer interfacial energy is dominant.

Concentric domain patterns resembling multilayered micelles and vesicles exhibit bifurcations wherein they only exist for sufficiently small dimensionless interfacial energies. The bifurcation of large radii vesicle solutions is studied analytically, and a crossover from a supercritical case with only one solution branch to a subcritical case with two is observed. Linearized stability of these configurations shows that azimuthal perturbation may lead to instabilities as interfacial energy is decreased.

Introduction

Block copolymers are molecularly bonded mixtures of two or more distinct polymer species, which may exhibit *microphase segregation*, wherein small domains of heterogeneous composition form. In the presence of a partially immiscible third phase, the mixture may also undergo *macrophase segregation*. The combined effect of both types of phase segregation leads to a wide variety of morphologies [1, 2, 3, 4, 5, 6].

Many of the basic patterns which form in these systems can be described as equilibria composed of alternating layers of polymer composition, surrounded by a solvent phase [7, 8, 3, 6]. In this paper, we study three morphological classes, shown in figure 1. The first of these are flat structures with many layers, referred to here as *lamellar multilayers*. These can be regarded as the multidimensional extension of one dimensional equilibria. In addition, there are two concentric equilibria types, which in analogy to amphiphilic chemical systems will be referred to as *micelles* and *vesicles*. The latter type has a solvent core, whereas the former does not.

This paper studies a dynamic free boundary problem which arises as the sharp interface limit of a density functional model. Density functional approaches have a long history in modelling heterogeneous polymer mixtures (e.g. [9, 10, 11]), and are a natural extension of the Cahn-Hilliard theory of phase separation [12]. The particular formulation we begin with was considered by Ohta

[*]Corresponding Author: Department of Mathematics, University of Arizona, Tucson AZ 85721 USA, Email: kglasner@math.arizona.edu

[†]Department of Mathematics, Duke University, Durham NC 27704 USA, Email: sorizaga@math.duke.edu

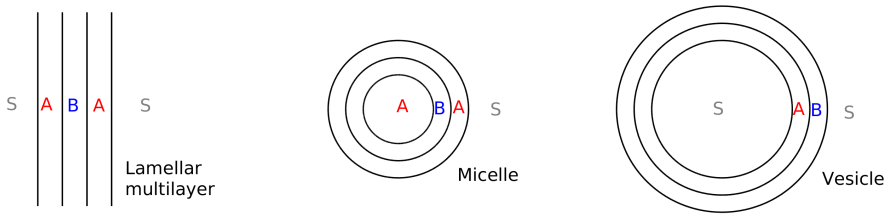

Figure 1: The three types of configurations studied in this paper. The number of alternating polymer domains N can be any integer ≥ 2.

and Ito [3]. The corresponding free boundary problem may be regarded as an extension of both the classic Mullins-Sekerka problem (e.g.[13]) and the two-phase free boundary evolution for block copolymers formulated by Nishiura and Ohnishi [14].

Localized multilayered block copolymer morphologies have been actively studied in recent years [15, 16, 17, 18, 19, 20]. Ohta and Nonomura [17] performed numerical studies of the density functional model used here and computed approximations to free energies of flat and concentric equilibria. Lamellar equilibria in a sharp interface model of copolymer-homopolymer blends were studied by van Gennip and Peletier [19, 20]. They rigorously establish the existence of mass-conserving energy minimizers and study stability through the second variation of the energy functional.

Concentric equilibria in block copolymer mixtures have also been studied previously. Ren and Wei [16] rigorously established the existence of radially symmetric patterns in a two phase model. More recently, Avalos et al. [21] studied a density functional model similar to the one discussed here. They numerically compute a variety of equilibria, including concentric micelle-type patterns. In addition, they compare their results to experimental observations of similar structures (e.g. [22]).

The starting point for our analysis is a dynamic free boundary problem which represents a singular limit of a density functional model. Some aspects of this model and its derivation are discussed in section 1. In section 2, the equilibrium lamellar multilayer morphology is studied. Analytic evidence is presented for large wavelength transverse instabilities. Stability with respect to arbitrary wavenumber perturbations is also studied by formulating a finite dimensional eigenvalue problem. Concentric equilibria are discussed in section 3. A hybrid analytical-numerical shooting method is used to compute equilibria and locate their bifurcations. For the micelle case, two solution branches merge in a fold bifurcation, whereas in the vesicle case the branch of large radii solutions can be analytically shown to emerge from lamellar multilayer equilibria. Azimuthal stability of concentric equilibria is studied by formulating an eigenvalue problem analogous to the lamellar case.

1 Density functional models and their sharp interface limit

Density functional models for block copolymer mixtures construct a free energy as a function of composition variables, here ϕ_A, ϕ_B, and ϕ_S, corresponding to copolymer constituents A and B, and a solvent phase S. One of these variables can be eliminated by invoking the standard assumption of incompressibility $\phi_A + \phi_B + \phi_S = 1$, which leads to a convenient reformulation [17] employing the variables

$$\Phi = (1-f)\phi_A - f\phi_B, \quad \Psi = f\phi_A + (1-f)\phi_B. \tag{1}$$

The parameter $f \in (0,1)$ is the fraction of A-monomer relative to the total polymer volume. It is assumed that these are finite, and it follows that

$$\int_{\mathbb{R}^d} \Phi \, dx = 0. \tag{2}$$

The resulting free energy functional can be written (in suitable dimensionless variables)

$$F = \int_{\mathbb{R}^d} \frac{1}{\epsilon} W(\Phi,\Psi) + \frac{\epsilon}{2}|\nabla\Phi|^2 + \frac{\epsilon}{2}|\nabla\Psi|^2 dx + \frac{\alpha}{2}\int_{\mathbb{R}^d}\int_{\mathbb{R}^d} G(x,x')\Phi(x)\Phi(x')\,dx\,dx'. \tag{3}$$

The nonlocal term has an interaction kernel $G()$, which is taken to be the Laplacian Green's function here. The potential $W(\Phi,\Psi)$ has minima at $(\Phi,\Psi) = (0,0)$, corresponding to pure solvent, and $(\Phi,\Psi) = (1-f,f)$ and $(-f,1-f)$, corresponding to pure A or B monomer, respectively. Dynamics are built from the assumption that diffusion is driven by gradients of the generalized chemical potentials $\mu = \delta F/\delta\Phi, \nu = \delta F/\delta\Psi$, leading to

$$\epsilon\Phi_t = \Delta\mu - \epsilon\alpha\Phi, \quad \mu \equiv -\epsilon^2\Delta\Phi + W_\Phi(\Phi,\Psi) \tag{4}$$

$$\epsilon\Psi_t = \Delta\nu, \quad \nu \equiv -\epsilon^2\Delta\Psi + W_\Psi(\Phi,\Psi). \tag{5}$$

While more general diffusive dynamics are possible, our primary interest is in linear stability, which is a function of energy and not kinetics.

1.1 Free boundary problem

The singular limit $\epsilon \to 0$ may be obtained by matched asymptotic expansions in the usual way (e.g. [13, 14, 23]). Some details are provided in the appendix for completeness. The result is a free boundary problem which describes the evolution of interfaces between three (open) domains $\Omega_A, \Omega_B, \Omega_S$, which correspond to the three minima of W, $(\Phi_0,\Psi_0) = (0,0)$, $(1-f,f)$ and $(-f,1-f)$, respectively. By virtue of (2), these subregions satisfy

$$\frac{|\Omega_A|}{f} = |\Omega_A \cup \Omega_B| = \frac{|\Omega_B|}{1-f}. \tag{6}$$

The normal interface velocities V_n are prescribed by the system

$$\Delta v = \begin{cases} 0, & x \in \Omega_S \\ 1-f, & x \in \Omega_A \\ -f, & x \in \Omega_B \end{cases} \tag{7}$$

$$\Delta w = 0, \quad x \in \Omega_S \cup \Omega_A \cup \Omega_B, \tag{8}$$

$$v\,[\Phi_0]^+_- + w\,[\Psi_0]^+_- = -\kappa\sigma_{pq}, \quad x \in \partial\Omega_{pq}, \quad p,q \in \{A,B,S\}, \tag{9}$$

$$[v]^+_- = 0 = [w]^+_-, \tag{10}$$

$$V_n = -\left[\partial v/\partial n\right]^+_- / \left[\Phi_0\right]^+_- = -\left[\partial w/\partial n\right]^+_- / \left[\Psi_0\right]^+_-. \tag{11}$$

The notation $[]^+_-$ refers to the jump of values across the interface. By convention, the normal to the interface will be oriented in the arbitrarily prescribed + direction, so that the interface curvature κ is positive if the phase corresponding to $-$ is locally convex. In some cases, $[\Psi_0]^+_- = 0$, and the last equality in (11) is replaced with $[\partial w/\partial n]^+_- = 0$.

The field variables v and w are the sharp interface, nondimensional versions of chemical potentials μ and ν defined in (4-5). As in the classical Cahn-Hilliard theory, the interface motion (11)

arises from a discontinuity of diffusive fluxes which derive from gradients of chemical potentials. Notice that there are two expressions for interface velocity, which seems to make the system overdetermined. On the other hand, the curvature boundary condition (9) and the continuity boundary conditions (10) are not linearly independent. As a consequence, there is an extra degree of freedom in solving the elliptic equations (7) and (8) which is removed by the self-consistency of the two velocity expressions in (11).

The system (7-11) has been written in dimensionless variables. The nondimensional surface energy parameters

$$\sigma_{pq} = \Sigma_{pq}\nu_\infty^{-3/2}\alpha^{1/2}, \quad p, q \in \{A, B, S\}, \tag{12}$$

will play a significant role in both bifurcation and stability. Here Σ_{pq} refers to the dimensional surface energy of the Ω_p-Ω_q interface, and ν_∞ is a prescribed characteristic chemical potential. We shall later impose far field conditions which specify ν_∞.

In addition to the free boundary equations above, one expects a Herring-type formula at three phase junctions [23]. The configurations we study have no such interface junctions, however, and these conditions may be ignored.

1.2 Far field conditions

The primary interest of this paper is the study of localized configurations which are in equilibrium with their environment, which is taken to be a homogeneous mixture of solvent and polymer. In the continuum equations, these lead to

$$\lim_{|x|\to\infty} \mu = 0, \qquad \lim_{|x|\to\infty} \nu = \epsilon\nu_\infty. \tag{13}$$

The first encodes the fact that far from the localized domains of interest, there is a perfectly homogeneous mixture and no preponderance of A or B phases. The second condition provides an ambient chemical potential, equivalent to specifying the dilute volume fraction of polymer in the far field.

The dynamic free boundary problem (7-11) does not capture the diffusive behavior of either Φ or Ψ far away. As explained in the appendix, there is necessarily a slowly varying "diffusion" layer using the stretched coordinate $X = \epsilon^{1/2}x$, valid for $X \gg \epsilon^{-1/2}$. Our interest here, however, is studying the stability of domain structures subject only to localized perturbations. This allows us to ignore dynamics in the diffusion layer, and use the effective far field conditions

$$\nabla v = O(r^{-d}) = \nabla w, \quad |x| \to \infty, \tag{14}$$

which prevents flux to and from infinity (see also the discussion in section 4). For the equilibrium problem, on the other hand, there is no diffusion layer for ν, and the scaled free boundary problem satisfies

$$\lim_{|x|\to\infty} w = 1. \tag{15}$$

For the lamellar structures considered in section (2), the limits in (14,15) only pertain to the first independent variable (i.e. x rather than y or z).

1.3 Volume conservation and energy dissipation

The free boundary problem (7-11) has two useful properties which provide some intuition about the interface evolution. The first is that volume $|\Omega_A \cup \Omega_B|$ of the polymer domains is conserved

provided (14) is invoked. This is seen by first noting that (6) implies

$$\int_{\mathbb{R}^d} \Psi_0 \, dx = \Big(f^2 + (1-f)^2 \Big) |\Omega_A \cup \Omega_B|. \tag{16}$$

Then conservation of the integral of Ψ_0 follows by

$$\frac{d}{dt} \int_{\mathbb{R}^d} \Psi_0 \, dx = \int_I [\Psi_0]^+_- V_n \, dx = \int_I [\partial w / \partial n]^+_- \, dx = 0, \tag{17}$$

where I refers to the collection of all interfaces. The final equality is a result of cancellation on shared interfaces, as well as the divergence theorem applied to the far field region.

The sharp interface version of energy (3) can written as the sum $E = E_p + E_s$, where E_p is the energy of polymer stretching

$$E_p = \frac{1}{2} \int_{\mathbb{R}^d} |\nabla u|^2 \, dx, \quad \Delta u = \Phi_0, \quad \lim_{x \to \infty} u = 0, \tag{18}$$

and E_s is the total surface energy

$$E_s = \sum_{p,q \in \{A,B,S\}} \sigma_{pq} |\partial \Omega_{pq}|. \tag{19}$$

One may regard $E = E(\Omega_A, \Omega_B)$ as a functional over a class of admissible states, which may be characterized as a pair of bounded, open domains $\Omega_{A,B} \subset \mathbb{R}^n$ with smooth boundaries which satisfy the volume fraction constraint $|\Omega_A|/|\Omega_B| = f/(1-f)$. For lamellar configurations, $\Omega_{A,B}$ should instead be regarded as subsets of a semi-infinite domain with cylindrical topology, i.e. a domain which is periodic in the longitudinal direction so that energy is finite.

It can be shown that the total energy is dissipated under the dynamics given by (7-11). A standard computation gives

$$\frac{dE}{dt} = \int_I \left(u[\Phi_0]^+_- + \sigma \kappa \right) V_n \, dx \tag{20}$$

where $\sigma = \sigma_{pq}$ is the surface energy on the pq-component of I. Introducing $J \equiv u - v$, the dissipation of energy is therefore

$$\begin{aligned}
\frac{dE}{dt} &= \int_I \Big(J - w[\Psi_0]^+_- / [\Phi_0]^+_- \Big) [\partial v / \partial n]^+_- \, dx && (21) \\
&= \int_{\mathbb{R}^d} \nabla v \cdot \nabla J + J \Delta v \, dx - \int_I w [\partial w / \partial n]^+_- \, dx && (22) \\
&= \int_{\mathbb{R}^d} \nabla (u - J) \cdot \nabla J + J \Delta u - |\nabla w|^2 \, dx && (23) \\
&= - \int_{\mathbb{R}^d} |\nabla J|^2 + |\nabla w|^2 \, dx. && (24) \\
& && (25)
\end{aligned}$$

Here the first line uses (9), the second line uses the second equality in (11), and Green's identity is used throughout.

2 Lamellar multilayered equilibria

We begin by considering the simplest morphology, one dimensional states composed of alternating blocks of the form $S|A|B|\ldots|A|S$ or $S|A|B\ldots|B|S$. The existence of these types of steady states and their stability was studied in a somewhat more general model in [20]. The present model is a limiting case (essentially for small ν_∞) of that formulation.

One dimensional equilibria can also be regarded as multidimensional equilibria. Here the linearized growth rates associated with longitudinal perturbations are computed. We find that for sufficiently large surface energies, multilayered configurations are stable for all longitudinal wavenumbers.

2.1 Equilibrium in one dimension

For the system domain $x \in \mathbb{R}$, the field equations (7,8) can be integrated explicitly to give a unique solution with interfaces at $x_0, x_1, ..., x_N$, where subintervals (x_j, x_{j+1}) represent domains Ω_A and Ω_B for j even or odd, respectively. This solution can be written in a compact manner by defining the domain widths (or half widths) by

$$l_0 = x_1 - x_0, \quad l_{N-1} = x_N - x_{N+1}, \quad l_j = (x_{j+1} - x_j)/2, \quad 1 \le j \le N-2, \tag{26}$$

where it is found that

$$l_j = \begin{cases} \frac{\sqrt{4f^2-4f+2}}{1-f} & j \text{ even} \\ \frac{\sqrt{4f^2-4f+2}}{f} & j \text{ odd} \end{cases} \tag{27}$$

By setting

$$\bar{x}_0 = x_0, \quad \bar{x}_{N-1} = x_N, \quad \bar{x}_j = (x_{j+1} + x_j)/2, \quad 1 \le j \le N-2, \tag{28}$$

the field variables are found to be $w \equiv 1$ and

$$v = v_0(x) \equiv \begin{cases} \frac{1-f}{2}(x - \bar{x}_j)^2 - \frac{f}{1-f}, & x_j < x < x_{j+1} \;\; j \text{ even}, \\ \frac{-f}{2}(x - \bar{x}_j)^2 + \frac{1-f}{f}, & x_j < x < x_{j+1} \;\; j \text{ odd}. \end{cases} \tag{29}$$

Before proceeding to discuss stability in multiple dimensions, we make a few comments about the one dimensional stability of this equilibrium. By virtue of the conservation and dissipation properties, our equilibrium may be regarded as a critical point of the energy $E = E_p(x_0, x_1, \ldots, x_N)$ subject to the constraint (16). This problem was considered by Ren and Wei [24] as the Γ-limit problem of the two phase diblock copolymer energy. It was shown that all N-layer one dimensional equilibria are in fact local energy minimizers. In our situation, this means that stability with respect to longitudinal perturbations is expected.

2.2 Dynamics of long wavelength disturbances

To investigate the evolution of weakly bent lamellar multilayers, the transverse variable is scaled $y' = \epsilon^{1/2} y$, and a timescale $t' = \epsilon t$ is used. The interfaces of the multilayered structure are regarded as graphs $x = \eta_j(y', t')$. The free boundary problem in the new coordinates is (after dropping

primes)

$$\epsilon v_{yy} + v_{xx} = \Phi_0, \quad \epsilon w_{yy} + w_{xx} = 0, \tag{30}$$

$$v\left[\Phi_0\right]_j + w\left[\Psi_0\right]_j = \epsilon\sigma_j\Big(\eta_{jy}/\sqrt{1+\epsilon\eta_{jy}^2}\Big)_y, \tag{31}$$

$$[w]_j = 0 = [v]_j\,, \tag{32}$$

$$\epsilon\eta_{jt}/\sqrt{1+\epsilon\eta_{jy}^2} = -[v_x + \epsilon v_y\eta_{jy}]_j/[\Phi_0]_j = -[w_x + \epsilon v_y\eta_{jy}]_j/[\Psi_0]_j. \tag{33}$$

Here σ_j is the surface energy associated with the j-th interface, $[]_j$ is the jump (oriented in the positive x direction) across the j-th interface.

The quantities v, w, η_j are expanded in powers of ϵ. The leading order solutions are simply those corresponding to the equilibrium multilayer with v_0 given by (29), $w_0 = 1$ and $\eta_{j0} = x_j$. The next order gives

$$v_{1xx} = 0 = w_{1xx}, \quad x \neq x_j \tag{34}$$

$$\Big(v_1(x_j) + v_{0x}(x_j)\eta_{j1}\Big)\left[\Phi_0\right]_j + w_1(x_j)\left[\Psi_0\right]_j = 0, \tag{35}$$

$$[w_1]_j = 0, \tag{36}$$

$$[v_{1x}]_j + \eta_{j1}[v_{0xx}]_j = 0 = [w_{1x}]. \tag{37}$$

It follows w_1 is continuously differentiable and therefore $w_1 = 0$. It is then easy to check that an explicit solution to (34-37) is $v_1 = -\eta v_{0x}$, where $\eta_{j1} \equiv \eta(y,t)$ are the same for all j.

The system for order ϵ^2 is

$$v_{2xx} = -\eta_{yy}v_{0x}, \quad w_{2xx} = 0, \quad x \neq x_j \tag{38}$$

$$\Big(v_2(x_j) + v_{0x}(x_j)\eta_{j2} - \frac{1}{2}v_{0xx}(x_j)\eta^2\Big)\left[\Phi_0\right]_j + w_2(x_j)\left[\Psi_0\right]_j = \sigma_j\eta_{yy}, \tag{39}$$

$$[w_2]_j = 0, \tag{40}$$

$$\eta_t = -\Big([v_{2x}]_j + [v_{0xx}]_j\eta_{j2}\Big)/\left[\Phi_0\right]_j = -[w_{2x}]/\left[\Psi_0\right]_j\,. \tag{41}$$

Solvability is obtained by multiplying the equation for v_2 by v_{0x}, integrating this by parts on each subinterval, and summing the results. This leads to

$$\eta_{yy}\int_{\mathbb{R}} v_{0x}^2 dx = \sum_{j=0}^{N} -v_{0x}(x_j)[v_{2x}]_j + \sigma_j\eta_{yy} - w_2(x_j)\left[\Psi_0\right]_j + \frac{1}{2}\left[\Phi_0^2\right]_j\eta^2 - v_{0x}(x_j)[v_{0xx}]_j\eta_{j2} \tag{42}$$

$$= \sum_{j=0}^{N} v_{0x}(x_j)\left[\Phi_0\right]_j\eta_t - w_2(x_j)\left[\Psi_0\right]_j + \sigma_j\eta_{yy}, \tag{43}$$

where the fact $\sum_{j=0}^{N}\left[\Phi_0^2\right]_j = 0$ was used. The solution $w_{2x} = -\eta_t\Psi_0$ can be obtained from integrating $w_{2xx} = 0$ and using condition (41). Then one calculates

$$\sum_{j=0}^{N} v_{0x}(x_j)\left[\Phi_0\right]_j = -\int_{\mathbb{R}}\Phi_0^2\,dx, \tag{44}$$

and

$$\sum_{j=0}^{N} w_2(x_j)\left[\Psi_0\right]_j = -\sum_{j=0}^{N}\int_{\mathbb{R}}(w_2\Psi_0)_x dx = \eta_t\int_{\mathbb{R}}\Psi_0^2\,dx. \tag{45}$$

Then (42) is nothing more than the diffusion equation

$$I\eta_t = D\eta_{yy}, \quad I = \int_{\mathbb{R}} \Phi_0^2 + \Psi_0^2 \, dx, \quad D = \sum_{j=0}^{N} \sigma_j - \int_{\mathbb{R}} v_{0x}^2 \, dx. \tag{46}$$

The threshold for long wavelength instabilities is $D = 0$, which represents a plane in σ_{AB}-σ_{AS}-σ_{BS} parameter space (see figures 3 and 4).

2.3 The linearized free boundary problem

To investigate finite wavelength instabilities, the complete linearization of the multidimensional free boundary problem is formulated. The perturbed interfaces are described as graphs $x = x_j + \tilde{x}_j(y,t)$ where $\tilde{x}_j$ is assumed small. The interface curvatures are approximated $\kappa_j \approx \partial^2 \tilde{x}_j / \partial y^2$, whose sign implies that the + side of each interface in the boundary conditions corresponds to $x > x_j$.

The field variables v and w are expanded $v(x,y) = v_0 + \tilde{v}$ and $w(x,y) = w_0 + \tilde{w}$, which solve

$$\Delta \tilde{v} = 0, \quad \Delta \tilde{w} = 0, \tag{47}$$

and the boundary conditions (9,10) expand to give

$$\big(v_{0x}(x_j)\tilde{x}_j + \tilde{v}(x_j,y)\big)[\Phi_0]_-^+ + \tilde{w}(x_j,y)[\Psi_0]_-^+ = \sigma_j \frac{\partial^2 \tilde{x}_j}{\partial y^2} \tag{48}$$

$$[\tilde{v}]_-^+ = 0 = [\tilde{w}]_-^+. \tag{49}$$

The linearized interface velocity (11) for the j-th interface is obtained from expanding the normal derivatives as $\partial v / \partial n = v_{0xx}(x_j)\tilde{x}_j + \tilde{v}_x(x_j)$. Using the fact $[v_{0xx}]_j = -[\Phi_0]_j$, this produces

$$\tilde{x}_{jt} + \tilde{x}_j = [\tilde{v}_x]_j / [\Phi_0]_j. \tag{50}$$

2.4 Large solvent-polymer surface energies

In general, the linear system (47,48,50) admits only a partial analytical solution, and the complete calculation requires numerical solution of an eigenvalue problem. The limit where $\sigma_{AS}, \sigma_{BS} \gg \sigma_{AB}$ is somewhat more tractable, and is useful to illustrate the crossover between long wavelength and small wavelength instabilities. In this case, the edge interfaces are essentially immobile so $\tilde{x}_0, \tilde{x}_N \approx 0$, and only the interior AB-interfaces play a role in the instability.

Consider the case $N = 2$, where $\tilde{x}_{0,2} \approx 0$, and $\tilde{x}_1 = \cos(ky)$. By virtue of (50), the perturbed fields $\tilde{v}, \tilde{w}$ are continuously differentiable across x_0 and x_2, so that

$$\tilde{v} = A\cos(ky) \begin{cases} e^{kx} & x < 0, \\ e^{-kx} & x > 0, \end{cases} \tag{51}$$

$$\tilde{w} = B\cos(ky) \begin{cases} e^{kx} & x < 0, \\ e^{-kx} & x > 0. \end{cases} \tag{52}$$

The conditions (48) and (50) give

$$-k^2\sigma_{AB} = -(A + v_0'(x_1)) + B(1-2f), \tag{53}$$

$$\lambda = -2Ak - 1 = \frac{2Bk}{1-2f}. \tag{54}$$

This system yields the growth rate

$$\lambda = \frac{2k\sqrt{4f^2-4f+2} - 2\sigma_{AB}k^3 - 1}{1+(1-2f)^2}. \tag{55}$$

A finite wavelength instability at wavenumber k^* is incipient at the value $\sigma_{AB} = \sigma^*_{AB}$. Setting $\lambda(k^*) = \lambda'(k^*) = 0$ we find

$$k^* = \frac{3}{4\sqrt{4f^2-4f+2}}, \quad \sigma^*_{AB} = \frac{16}{27}(4f^2-4f+2)^{3/2}. \tag{56}$$

This compares favorably with the vertical asymptotes of the curves in figure 3.

A similar calculation can be done in the case $N = 3$, where $\tilde{x}_{0,3} \approx 0$, and $\tilde{x}_{1,2} = \cos(ky)$. With $x_2 = -x_1 = \sqrt{4f^2-4f+2}$, the field variables $\tilde{v}, \tilde{w}$ can be found as

$$\tilde{v} = A\cos(ky)\begin{cases} e^{kx} & |x| > x_2, \\ e^{-kx}\cosh(kx)/\cosh(kx_1) & |x| < x_2, \end{cases} \tag{57}$$

$$\tilde{w} = B\cos(ky)\begin{cases} e^{kx} & |x| > x_2, \\ e^{-kx}\cosh(kx)/\cosh(kx_1) & |x| < x_2. \end{cases} \tag{58}$$

$$\tag{59}$$

Conditions (48) and (50) yield

$$-k^2\sigma_{AB} = -Ae^{kx_1} - v_{0x}(x_1) + Be^{kx_1}(1-2f), \tag{60}$$

$$\lambda = -2Ake^{kx_1}(\tanh(kx_1)-1) - 1 = \frac{2Bk}{1-2f}, \tag{61}$$

and elimination as before gives the growth rate

$$\lambda = \frac{[\tanh(kx_1)-1](\sigma_{AB}k^3 - k\sqrt{4f^2-4f+2}) - 1}{1+(1-2f)^2}. \tag{62}$$

The conditions for onset of a finite wavelength instability in this case lead to transcendental equations. For $f = 1/2$, for example, one finds $k^* = 0.81$ and $\sigma^*_{AB} = 0.55$, which compares favorably to figure 4.

2.5 Transverse instability for arbitrary wavenumbers

Exact solutions to the linearized free boundary problem (47,48,50) are now computed. For perturbations which do not grow as $|y| \to \infty$, it is sufficient to consider modes of the form

$$\tilde{x}_j = X_j e^{\lambda t}\cos(ky), \quad j = 0, 1, \ldots, N \tag{63}$$

where $k > 0$. The solutions for $\tilde{w}$ an $\tilde{v}$ can be explicitly constructed as

$$\tilde{v} = (V^+_m e^{kx}\cos(ky) + V^-_m e^{-kx}\cos(ky))e^{\lambda t} \tag{64}$$

$$\tilde{w} = (W^+_m e^{kx}\cos(ky) + W^-_m e^{-kx}\cos(ky))e^{\lambda t} \tag{65}$$

for each subregion $x_{m-1} < x < x_m$ where $m = 0, 1, .., N+1$. In writing this, we define $x_{-1} = -\infty$ and $x_{N+1} = +\infty$. By virtue of the far field conditions, $V^-_0 = 0 = W^-_0$ and $V^+_{N+1} = 0 = W^+_{N+1}$.

Inserting (63,64,65) into (48-49) gives linear relations for each $j = 0, 1, 2, \ldots, N$ of the form

$$(V_m^+ e^{kx_j} + V_m^- e^{-kx_j})[\Phi_0]_j + (W_m^+ e^{kx_j} + W_m^- e^{-kx_j})[\Psi_0]_j = -\Big(\sigma_j k^2 + v_{0x}(x_j)\Big)X_j, \quad m = j, j+1 \tag{66}$$

$$V_j^+ e^{kx_j} + V_j^- e^{-kx_j} = V_{j+1}^+ e^{kx_j} + V_{j+1}^- e^{-kx_j}, \tag{67}$$

$$W_j^+ e^{kx_j} + W_j^- e^{-kx_j} = W_{j+1}^+ e^{kx_j} + W_{j+1}^- e^{-kx_j}, \tag{68}$$

where $\sigma_j, [\Phi_0]_j, [\Psi_0]_j$ are the corresponding values at the unperturbed interfaces $x = x_j$. Since one of the relations (66-68) is redundant, it can be seen that (66-68) represent $4 + 4N$ equations for the $4 + 4N$ unknowns $V_j^\pm$ and $W_j^\pm$. These can be written in matrix-vector notation as $\boldsymbol{LC} = \boldsymbol{BX}$ where $\boldsymbol{C} = (V_0^+, W_0^+, \ldots, V_{N+1}^-, W_{N+1}^-)^T$, $\boldsymbol{X} = (X_0, X_1, \ldots, X_N)$, and $\boldsymbol{L}$ is square and invertible.

The linearized interface velocity (50) leads to

$$k(V_{j+1}^+ e^{kx_j} - V_{j+1}^- e^{-kx_j} - V_j^+ e^{kx_j} + V_j^- e^{-kx_j})/[\Phi_0]_j = (\lambda + 1)X_j, \quad j = 0, 1, \ldots, N, \tag{69}$$

which can be written in matrix form as $\boldsymbol{MC} = (\lambda + 1)\boldsymbol{X}$. It follows that the linearized growth rates formally satisfy the eigenvalue problem

$$\boldsymbol{ML}^{-1}\boldsymbol{BX} = (\lambda + 1)\boldsymbol{X}. \tag{70}$$

This problem is solved numerically.

Using the lamellar equilibrium solutions in section (2), it is possible to compute the maximum eigenvalue λ_{max} as a function of wavenumber k and other system parameters. A typical result is shown in figure 2. Significantly, stability of lamellar structures appears to be more likely for larger surface energies.

The neutral stability curves in surface energy parameter space given by $\lambda_{max} = 0$ are plotted in figure 3 for the case $N = 2$. These curves coincide with the long wavelength results (dotted lines) when the surface energy σ_{AB} is dominant. In the opposite case where the edge surface energies dominate, our earlier predictions about instability are also corroborated. The modes of instabilities can be further characterized using the eigenvectors associated with λ_{max} which allow us to uncover the amplitude at which each perturbed interface operates. The fastest growing modes are also shown in figure 3, also in agreement with earlier analytic predictions.

The neutral stability curves with $N = 3$ are also is presented in figure 4. The results are similar to the $N = 2$ case, with long wavelength instability dominant when $\sigma_{AB} \gg \sigma_{AS}$, and finite wavelength instability dominant when $\sigma_{AB} \ll \sigma_{AS}$.

The case of larger numbers of layers was also investigated. Figure 5 shows neutral stability curves as a function of surface energy for the cases $N = 2, 3, 4, 5$. Notice that instability is more prevalent as the number of interfaces increases.

2.6 Nonlinear evolution

Here we briefly illustrate the evolution of the morphology in the case where a lamellar multilayer is unstable. In principle, a weakly nonlinear analysis might capture certain aspects of this process. On the other hand, we generally find that instabilities represent subcritical bifurcation points, and the dynamics drives interfaces to a complex shape unobtainable by a perturbative analysis.

To approximate the free boundary evolution, we use the continuum equations (4-5). The potential employed has the form

$$W = A\phi_A^2(1 - \Phi_A)^2 + B\phi_B^2(1 - \Phi_B)^2 + C\phi_S^2(1 - \Phi_S)^2, \tag{71}$$

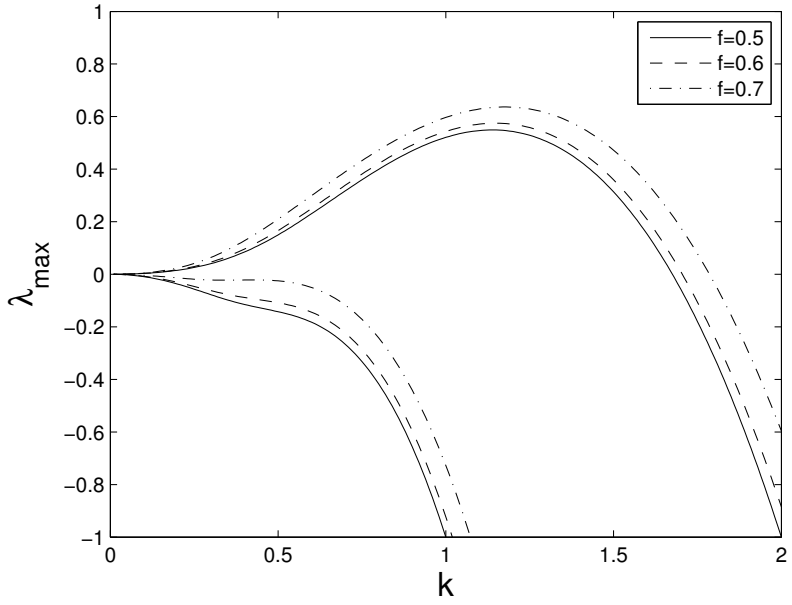

Figure 2: Maximum growth rates as a function of wavenumber k for various volume fractions ($N = 2$). The surface energies are $\sigma_{AS} = \sigma_{AB} = \sigma_{BS} = 1$ for the lower three curves, whereas they are all equal to 0.25 in the upper set of curves.

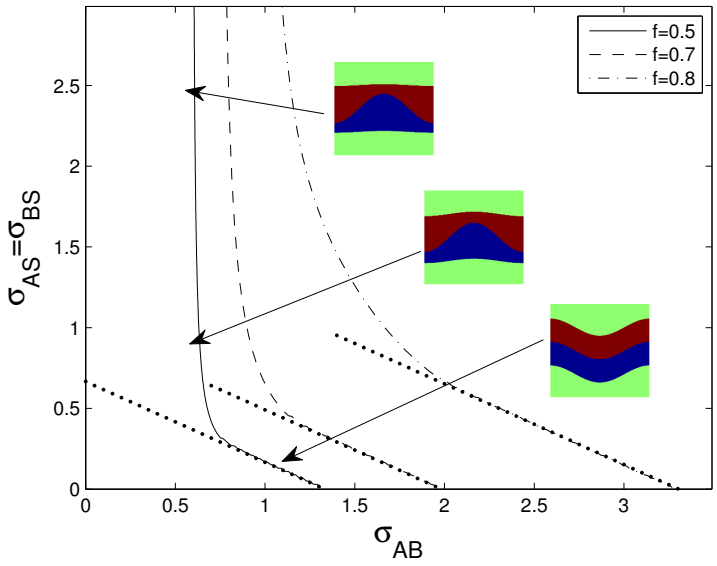

Figure 3: Neutral stability curves for the $N = 2$ in the space of surface energy parameters. The dotted line represents the neutral stability curve for long wavelength modes. Unstable modes are to the left of the curve and stable modes are to the right.

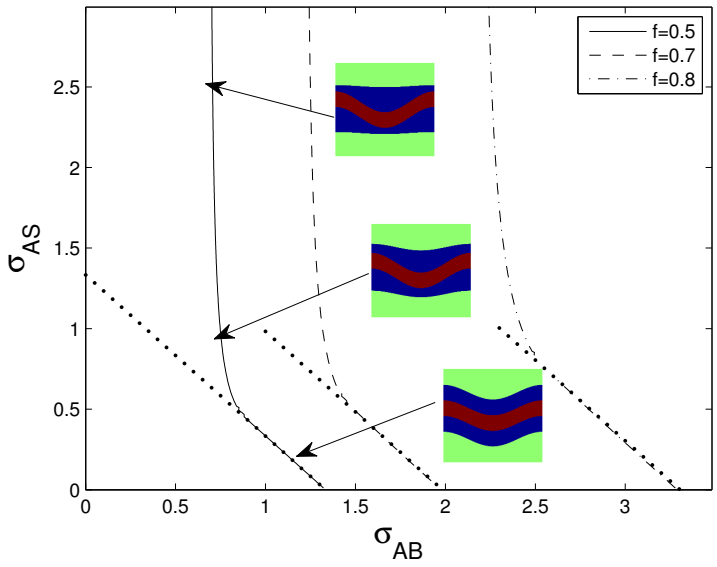

Figure 4: Neutral stability curves for the $N = 3$ case. The dotted line represents the neutral stability curve for long wavelength modes. Unstable modes are to the left of the curve and stable modes are to the right.

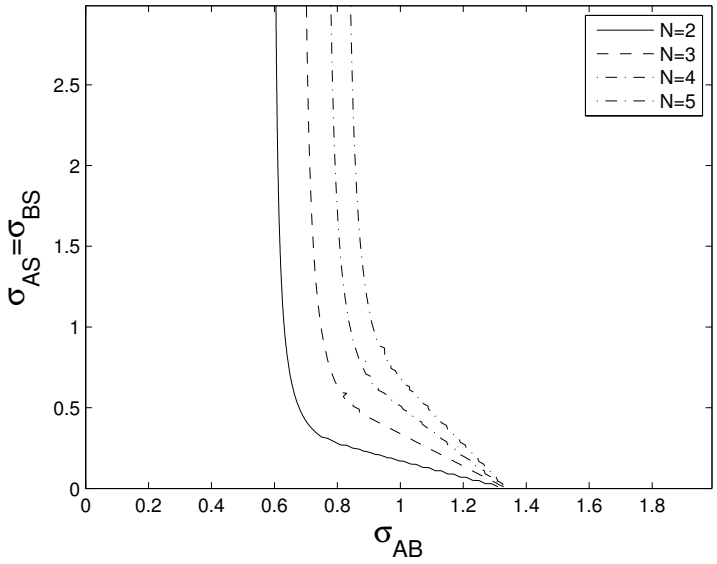

Figure 5: Neutral stability curves for various N-layered solutions. In all cases the volume fraction was $f = 0.5$.

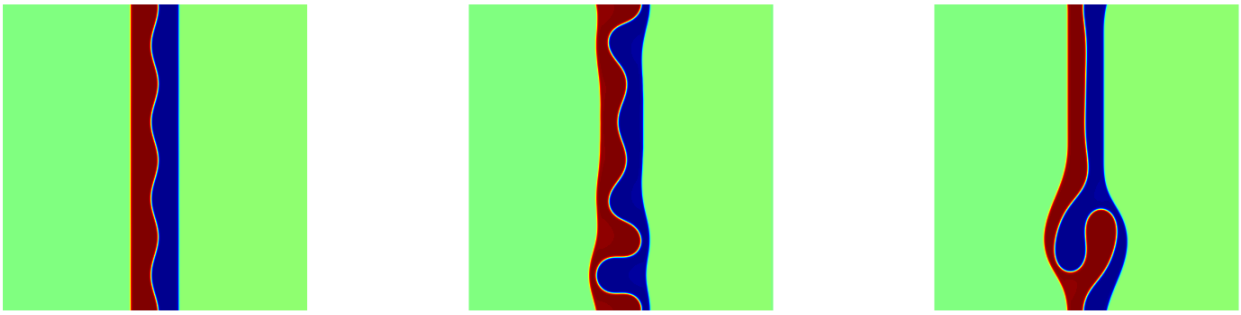

Figure 6: Evolution of an unstable multilayer ($N = 2$) with surface energies just below threshold. The final state (right) appears to be a stable equilibrium.

where the phase volume fractions are related to Φ and Ψ by (1). By explicitly computing the heteroclinic orbits that define the diffuse interface (see the appendix), we find that $A = 18.4 = B$ and $C = 65.6$ give roughly $\sigma_{AB} = \sigma_{AS} = \sigma_{BS} = 1$, for example.

Figure 6 shows the evolution of a barely unstable multilayer ($N = 2$,$f = 0.5$). To accomplish this, the potential was scaled so that all surface energies are 0.65, and a perturbed initial condition was provided by first computing a one dimensional equilibria. The computation was done on a 1024^2 grid using periodic boundary conditions. Other details of the numerical method are in [25].

Notably, the mode of instability is as predicted, with the outer interfaces much less mobile than the middle interface. As the magnitude of this mode grows, however, the periodic symmetry in the longitudinal direction is broken. This results in a straightening of the layered configuration over most of its length, and an undulation of interfaces at a single location. This process appears to equilibrate, creating a novel equilibrium structure.

3 Concentric equilibria

We now consider multilayered equilibria with radial symmetry in two and three dimensions. There are two qualitative cases to consider: *micelles*, which only have solvent on the exterior and *vesicles* which have a solvent core. In the former case, we suppose that the A-monomer domains are of the form $r_j < r < r_{j+1}$ where $r_0 = 0$ and j is even. The B-monomer domains are therefore of the form $r_j < r < r_{j+1}$ with j odd, and the solvent domain is $r > r_N$. The vesicle case is similar except $r_0 > 0$ and the solvent domain includes $r < r_0$.

In arbitrary dimension $d \geq 2$, the free boundary problem for concentric equilibria is

$$\Delta v = \begin{cases} 0 & r < r_0, \\ 1 - f & r_j < r < r_{j+1}, \quad j \text{ even}, \\ -f & r_j < r < r_{j+1}, \quad j \text{ odd}, \end{cases} \tag{72}$$

$$v(r_j) = \begin{cases} -(d-1)\sigma_{AB}/r_j + 1 - 2f, & 0 < j < N, \, j \text{ even}, \\ (d-1)\sigma_{AB}/r_j + 1 - 2f, & 0 < j < N \; j \text{ odd}, \end{cases} \tag{73}$$

$$v(r_N) = \begin{cases} (-(d-1)\sigma_{BS}/r_N + 1 - f)/(f), & N \text{ even}, \\ (-(d-1)\sigma_{AS}/r_N + f)/(f-1), & N \text{ odd}, \end{cases} \tag{74}$$

$$[v_r]_{r_j} = 0, \quad 0 < j < N, \qquad v_r(0) = 0 = v_r(r_N). \tag{75}$$

For the vesicle case, the innermost interface has the boundary condition

$$v(r_0) = ((d-1)\sigma_{AS}/r_0 + f)/(f-1). \tag{76}$$

The solution procedure we employ is hybrid analytical/numerical shooting method, which yields a function $S(r)$ whose zeros correspond to equilibrium values of r_1 for the micelle case or r_0 for the vesicle case. The solution to (72) together with (75a) is determined analytically layer by layer. The other boundary conditions are algebraically intractable and require numerical solution.

3.1 Micelles

For $0 < r < r_1$, equation (72) admits the solution

$$v(r) = \frac{1-f}{2d}(r^2 - r_1^2) + \sigma_{AB}/r_1 + 1 - 2f. \tag{77}$$

Provided r_1 is known, this completely determines the solution for $r < r_1$ and provides boundary conditions at r_1 for the domain $r_1 < r < r_2$. Proceeding inductively, $v(r)$ is determined on each interval $r_j < r < r_{j+1}$ for $j < N-1$, yielding

$$v(r) = \begin{cases} \frac{-f}{2d}(r^2 - r_j^2) + c_j G(r, r_j) + (d-1)\sigma_{AB}/r_j + 1 - 2f, & j \text{ odd} \\ \frac{1-f}{2d}(r^2 - r_j^2) + c_j G(r, r_j) - (d-1)\sigma_{AB}/r_j + 1 - 2f, & j \text{ even} \end{cases} \tag{78}$$

where $G(r, r_1) = \ln(r/r_1)$ for dimension $d = 2$ and $G(r, r_j) = 1/r_j - 1/r$ for $d = 3$. Using the condition (75) one has $c_1 = r_1^d/d$ and in general $c_{j+1} = c_j - (-1)^j r_j^d/d$.

The sequence of radii $r_2, r_3, ...$ can be found recursively by using the boundary conditions (74), noting that $r_{j+1} = \rho$ is a solution to

$$v(\rho) = R(\rho) \equiv \begin{cases} -(d-1)\sigma_{AB}/\rho + 1 - 2f, & j \text{ odd} \\ (d-1)\sigma_{AB}/\rho + 1 - 2f, & j \text{ even.} \end{cases} \tag{79}$$

Analytic solutions of (79) are either impossible or too cumbersome to be of value. On the other hand, it is possible to show that there is a unique solution with $\rho > r_j$, roughly as a result of monotonicity of each side of (79). When j is odd, for example, $v(r_j) > 1 - 2f$ and $v(\rho)$ is either decreasing to $-\infty$ for $\rho > r_j$ or has a single local maximum $r_{max} > r_j$ such that $v(\rho)$ will be decreasing to $-\infty$ for $\rho > r_{max}$. For the right hand side of (79), $R(r_j) = 1 - 2f$ and $R(\rho)$ is increasing as a function of ρ. A similar argument applies for j even. In practice, r_{j+1} is found numerically by simple bisection.

For the domain where $r > r_{N-1}$, the outermost radius r_N is found by invoking the last condition in (75), $v_r(r_N) = 0$, which leads to

$$r_N = \begin{cases} \left(\frac{dc_{N-1}}{f-1}\right)^{1/d}, & N \text{ odd}, \\ \left(\frac{dc_{N-1}}{f}\right)^{1/d}, & N \text{ even}. \end{cases} \tag{80}$$

At this point, we have constructed a function $v(r; r_1)$ so as to satisfy (72-75) except for the Dirichlet boundary condition at r_N. Moreover, induction on j shows that both $v(r; r_1)$ and the radii $r_j(r_1)$ are smooth functions of r_1. It follows that equilibrium solutions correspond to zeros of the smooth function

$$S(r_1) = \begin{cases} v(r_N; r_1) - (-(d-1)\sigma_{AS}/r_N + f)/(f-1), & N \text{ odd}, \\ v(r_N; r_1) - (-(d-1)\sigma_{BS}/r_N + 1 - f)/f, & N \text{ even}. \end{cases} \tag{81}$$

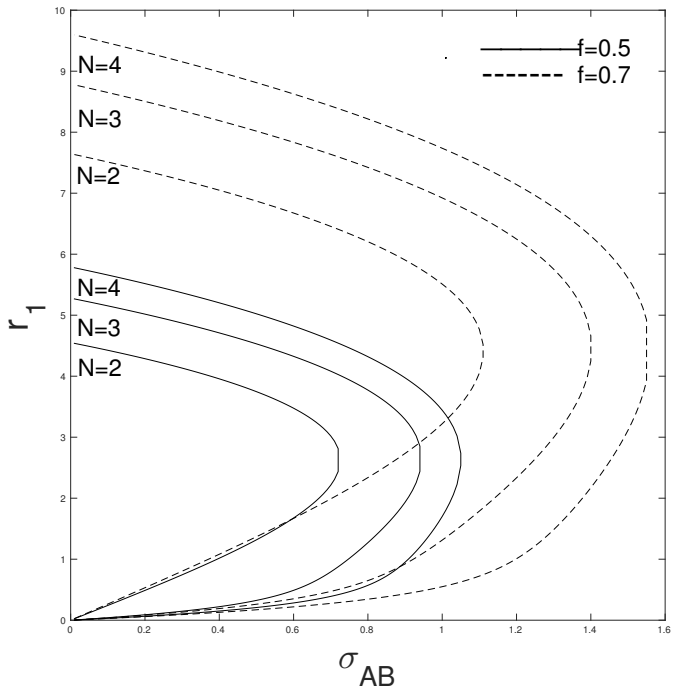

Figure 7: Equilibrium radii r_1 versus the surface energy parameter $\sigma_{AB} = \sigma_{AS} = \sigma_{BS}$, showing a fold bifurcation. The dimension is $d = 2$ in all cases; results for three dimensions look similar.

Numerical solutions using the procedure are shown in figure 7. In general, micelle equilibria only exist when surface energies are small enough. Two branches of solutions are observed, terminating in a fold bifurcation as one (or more) of the surface energy parameters is increased. Existence of these type of equilibria appear to be more likely as either the number of layers or the A-monomer volume fraction is increased.

3.2 Vesicles

The procedure outlined above can be modified in the situation where solvent occupies the innermost domain. In this case, for $r_0 < r < r_1$ equation (72) admits the solution

$$v(r) = \frac{1-f}{2d}(r^2 - r_0^2) + c_1 G(r, r_0) + ((d-1)\sigma_{AS} + f)/(f-1) \tag{82}$$

where $c_1 = (f-1)r_0^d/d$ by virtue of $v_r(r_0) = 0$. The remainder of the construction for $v(r)$ and r_j, $j = 1, 2, 3, \ldots, N$ is given above. Note this means that $v(r; r_0)$ and r_N are smooth functions of r_0, and so is the function $S(r_0)$, whose zeros in this case correspond to vesicle-type equilibria.

In contrast to the micelle case, $S(r_0)$ may have zero, one or two roots. The behavior of radii as a function of the surface energy parameter σ_{AB} is shown in figure 8. When all surface energies are set equal, we find that there in only one branch of solutions, terminating at infinite radius. In contrast, when the edge surface energy σ_{AS} is small, there may be two branches connected by a fold bifurcation.

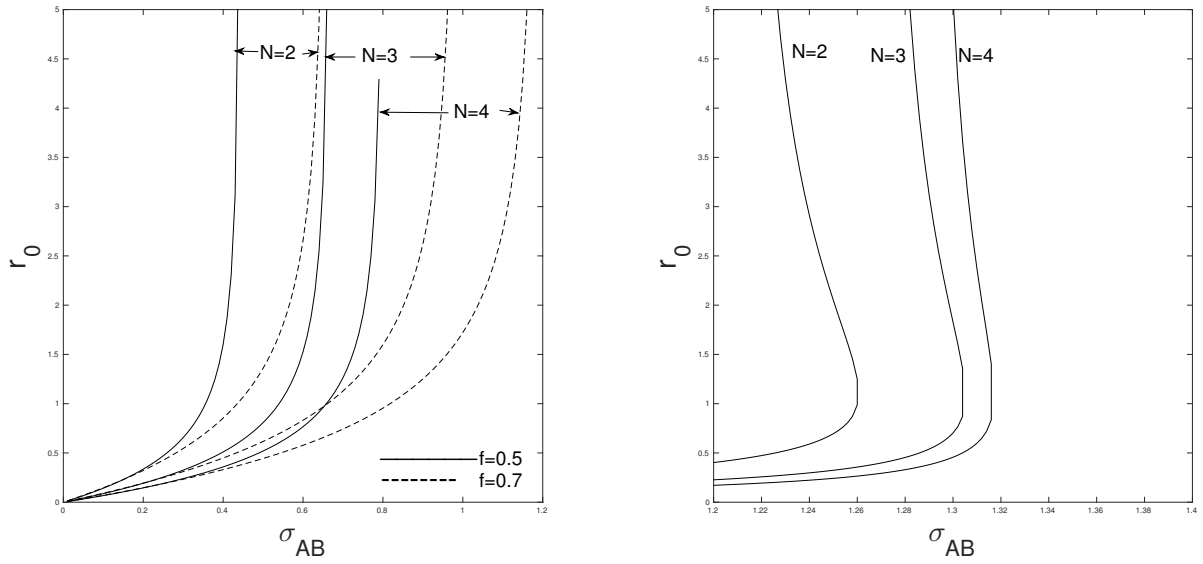

Figure 8: Equilibrium radii r_0 versus the surface energy parameter σ_{AB} ($d = 2$ in all cases). Left: when all surface energies are equal, there is only one branch of solutions. Right: When $\sigma_{AS} = \sigma_{AB}/20$ ($N = 3$), there may be two solution branches.

3.3 Large radii vesicles

Vesicle configurations whose interfaces have large radii may be regarded as weakly curved lamellar multilayers. For this reason, a perturbation expansion of (72-75) using the small parameter $\epsilon = 1/r_0$ is useful. This is done by expanding $v(r) = v_0(r) + \epsilon v_1(r) + \ldots$ and $r_j = r_0 + r_{j0} + \epsilon r_{j1} + \ldots$, where it is supposed that $r_{j0} = O(1)$. The surface tension values σ_j at each interface operate as bifurcation parameters, and they are expanded $\sigma_j = \sigma_{j0} + o(1)$. The values of σ_{j0} where the vesicle solution bifurcates from the straight lamellar one will be determined.

The leading order solution is the equilibrium multilayer with v_0 given by (29), and $r_{0j} = x_j$ are just the lamellar multilayer interface locations. The next order system is

$$v_1'' = (1-d)v_0', \tag{83}$$

$$v_1(r_0 + r_{j0}) + v_0'(r_0 + r_{j0})r_{j1} = (1-d)\sigma_j/[\Phi_0]_j, \tag{84}$$

$$[v_1']_j + [v_0'']_j r_{1j} = 0, \tag{85}$$

where as before $[]_j$ is the jump across the j-th interface. Solvability is obtained as in the discussion in section (2.2), by multiplying equation (83) by v_0', integrating this by parts on each subinterval, and summing. The result is

$$\Pi(\sigma_{AB}, \sigma_{AS}, \sigma_{BS}) = \Pi^* \equiv \int_{\mathbb{R}} v_0'^2 dr, \quad \Pi \equiv \sum_{j=0}^{N} \sigma_j, \tag{86}$$

which describes a codimension one surface in $(\sigma_{AB}, \sigma_{AS}, \sigma_{BS})$-parameter space. Comparing to (46), it follows that the threshold for long wavelength instability of the lamellar multilayer is precisely where large radii vesicles bifurcate.

Numerical evidence indicates a crossover from a supercritical situation, where a unique branch of vesicle solutions exist only when $\Pi < \Pi^*$ as in figure 8(left), to a subcritical one where two

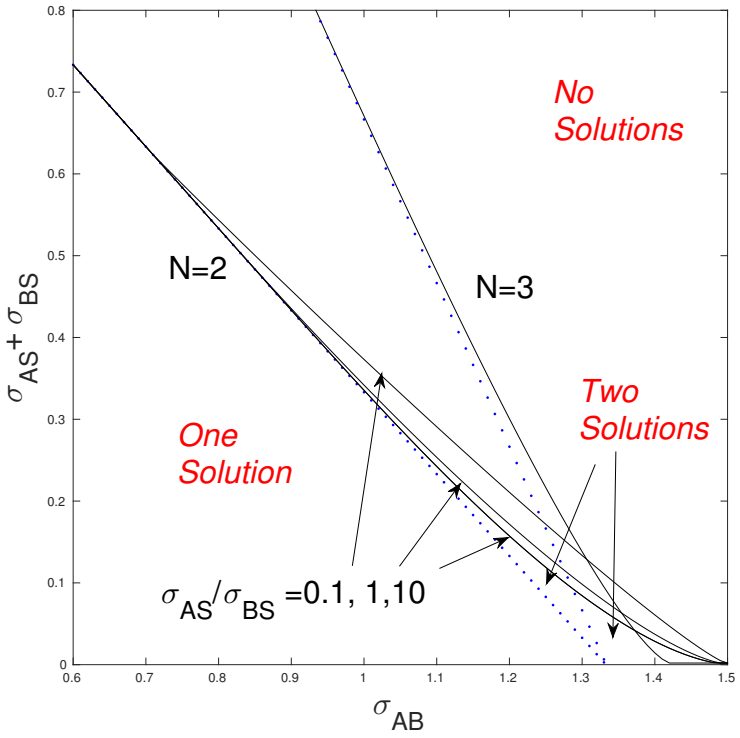

Figure 9: A phase diagram for vesicle equilibria as a function of σ_{AB} and the sum of the other two surface energies ($d = 2$ and $f = 1/2$). The dotted (blue) line indicates the infinite-radius bifurcation surface given by (86). The solid lines delineate the upper bound on surface energy for vesicle solutions to exist. When $\sigma_{AB} \gg \sigma_{AS} + \sigma_{BS}$, the bifurcation is supercritical and there is only one solution branch. On the other hand, when $\sigma_{AB} \ll \sigma_{AS} + \sigma_{BS}$, there may be two solution branches which exist above the infinite-radius bifurcation surface.

solution branches exist for $\Pi > \Pi^*$. A phase diagram showing this crossover is given in figure 9, showing regions in parameter space defined by the number of branches.

3.4 Stability of concentric equilibria

The stability of concentric equilibria is now considered, including both the possibility of radial and azimuthal perturbations. The formulation of the linearized problem is described for vesicles; the case of micelles is nearly identical.

For the two dimensional situation, the j-th deformed interface is described as a graph $r = r(\theta)$ where $r(\theta) = r_j + \tilde{r}_j(\theta, t)$ and $\tilde{r}_j$ is assumed small. As in the lamellar case, the field variables are also perturbed as $v(r, \theta) = v_0 + \tilde{v}$ and $w(r, \theta) = w_0 + \tilde{w}$, where $\Delta\tilde{v} = 0$ and $\Delta\tilde{w} = 0$. The linearized boundary condition (9) is

$$\big(v_{0r}(r_j)\tilde{r}_j + \tilde{v}(r_j, \theta)\big)[\Phi_0]_j + \tilde{w}(r_j, \theta)[\Psi_0]_j = \sigma_j \frac{\tilde{r}_j + \tilde{r}_{j\theta\theta}}{r_j^2} \tag{87}$$

and the linearized interface velocity (11) is

$$\tilde{r}_{jt} + \tilde{r}_j = [\tilde{v}_r]_j/[\Phi_0]_j. \tag{88}$$

It suffices to consider interface perturbations which are circular harmonics, leading to

$$\tilde{r}_j = R_j e^{\lambda t}\cos(n\theta), \quad j = 0, 1, \ldots, N \tag{89}$$

$$\tilde{v} = (V_m^+ r^n \cos(n\theta) + V_m^- r^{-n}\cos(n\theta))e^{\lambda t} \tag{90}$$

$$\tilde{w} = (W_m^+ r^n \cos(n\theta) + W_m^- r^{-n}\cos(n\theta))e^{\lambda t} \tag{91}$$

for each subregion $r_{m-1} < r < r_m$ where $m = 0, 1, .., N+1$. Similar to the lamellar case, we define $r_{-1} = 0$ and $r_{N+1} = +\infty$, which forces the field coefficients to be $V_0^- = W_0^- = 0$ and $V_{N+1}^+ = W_{N+1}^+ = 0$. In the case of radial perturbations where $n = 0$, The last two expressions (90) and (91) are replaced by

$$\tilde{v} = (V_m^+ + V_m^- G(r))e^{\lambda t} \tag{92}$$

$$\tilde{w} = (W_m^+ + W_m^- G(r))e^{\lambda t}, \tag{93}$$

where G is the Green's function, and $V_{N+1}^- = W_{N+1}^- = 0$ instead.

Using (89 - 91) in (87) and (88) produces linear relations

$$(V_m^+ r_j^n + V_m^- r_j^{-n})[\Phi_0]_j + (W_m^+ r_j^n + W_m^- r_j^{-n})[\Psi_0]_j = \Big(\sigma_j \frac{1-n^2}{r_j^2} - v_{0r}(r_j)[\Phi_0]_j\Big)R_j, \quad m = j, j+1 \tag{94}$$

$$n(V_{j+1}^+ r^{n-1} - V_{j+1}^- r^{-(n+1)} - V_j^+ r^{n-1} + V_j^- r^{-(n+1)})/[\Phi_0]_j = (\lambda+1)R_j, \quad j = 0, 1, \ldots, N. \tag{95}$$

Equations (94) and the continuity of $\tilde{w}$

$$W_j^+ r_j^n + W_j^- r_j^{-n} = W_{j+1}^+ r_j^n + W_{j+1}^- r_j^{-n} \tag{96}$$

form a a linear system of $4(N+1)$ equations and $4(N+1)$ unknowns. The remainder of the formulation is identical to the lamellar case, producing an eigenvalue problem of the form (70).

The three dimensional case has perturbations which are graphs

$$r = r_j + \tilde{r}_j(\theta, \phi, t), \tag{97}$$

where θ and ϕ are the azimuthal variables in spherical coordinates. In this case, it is sufficient to take interface deformations which are spherical harmonics $Y_l^m(\theta, \phi)$ leading to expressions

$$\tilde{r}_j = R_j e^{\lambda t} Y_l^m(\theta, \phi), \quad j = 0, 1, \ldots, N \tag{98}$$

$$\tilde{v} = (V_m^+ r^l Y_l^m(\theta, \phi) + V_m^- r^{-(l+1)} Y_l^m(\theta, \phi))e^{\lambda t} \tag{99}$$

$$\tilde{w} = (W_m^+ r^l Y_l^m(\theta, \phi) + W_m^- r^{-(l+1)} Y_l^m(\theta, \phi))e^{\lambda t} \tag{100}$$

Using the above expressions produces the linearized curvature boundary conditions and linearized normal velocity

$$(V_m^+ r_j^l + V_m^- r_j^{-(l+1)})[\Phi_0]_j + (W_m^+ r_j^l + W_m^- r_j^{-(l+1)})[\Psi_0]_j = -\Big(\sigma_j \frac{l(l+1)}{r_j^2} + v_{0r}(r_j)[\Phi_0]_j\Big)R_j, \quad m = j, j+1 \tag{101}$$

$$(V_{j+1}^+ l r^{(l-1)} - V_{j+1}^-(l+1)r^{-(l+2)} - V_j^+ l r^{(l-1)} + V_j^-(l+1)r^{-(l+2)})/[\Phi_0]_j = (\lambda+1)R_j, \quad j = 0, 1, \ldots, N, \tag{102}$$

The remainder of the formulation is the same as the case of two dimensions.

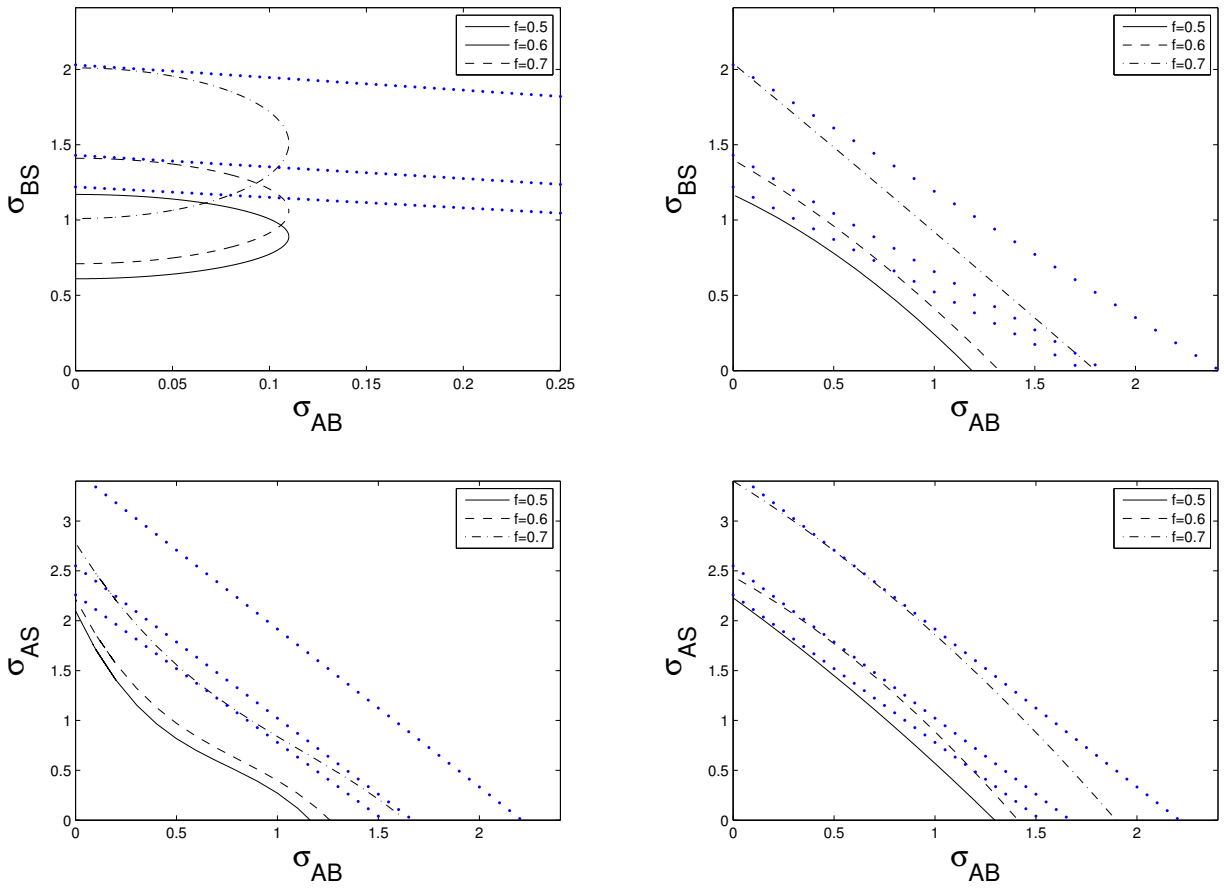

Figure 10: Two dimensional micelle neutral stability curves where $N = 2$ (top) and $N = 3$ (bottom). The figures to the left are for the small radii branch, and the figures to the right are the large radii branch of equilibria. The (blue) dotted lines represent the fold bifurcation, above which micelles will not exist. From bottom to top they correspond to $f = 0.5, 0.6, 0.7$, respectively.

The eigenvalue problems described above were solved numerically for a variety of parameters. Figure (10) shows neutral stability curves (black) for both small (left) and large (right) micelles in surface energy parameter space, where $N = 2, 3$. In the case $N = 2$, $\sigma_{AS} = \sigma_{BS}$. The dotted (blue) curves indicate the upper bound for existence, corresponding to the fold bifurcation in figure 7. Figure (11) shows the same type of plot for the three dimensional case. The region for instability of small micelles with $N = 2$ is inside the narrow oval regions. This suggests that two-layer micelles enjoy considerable stability and might be commonly observed structures, consistent with numerical simulations of the continuum equations [3].

In figure 12, the neutral stability curves for vesicle equilibria are shown, where $d = 2$ and $N = 2, 3$, together with the existence threshold (dotted). The situation in three dimensions is qualitatively similar. In light of the results of section 3.3, it appears that modestly curved vesicles are stable, but instabilities appear as the curvature increases.

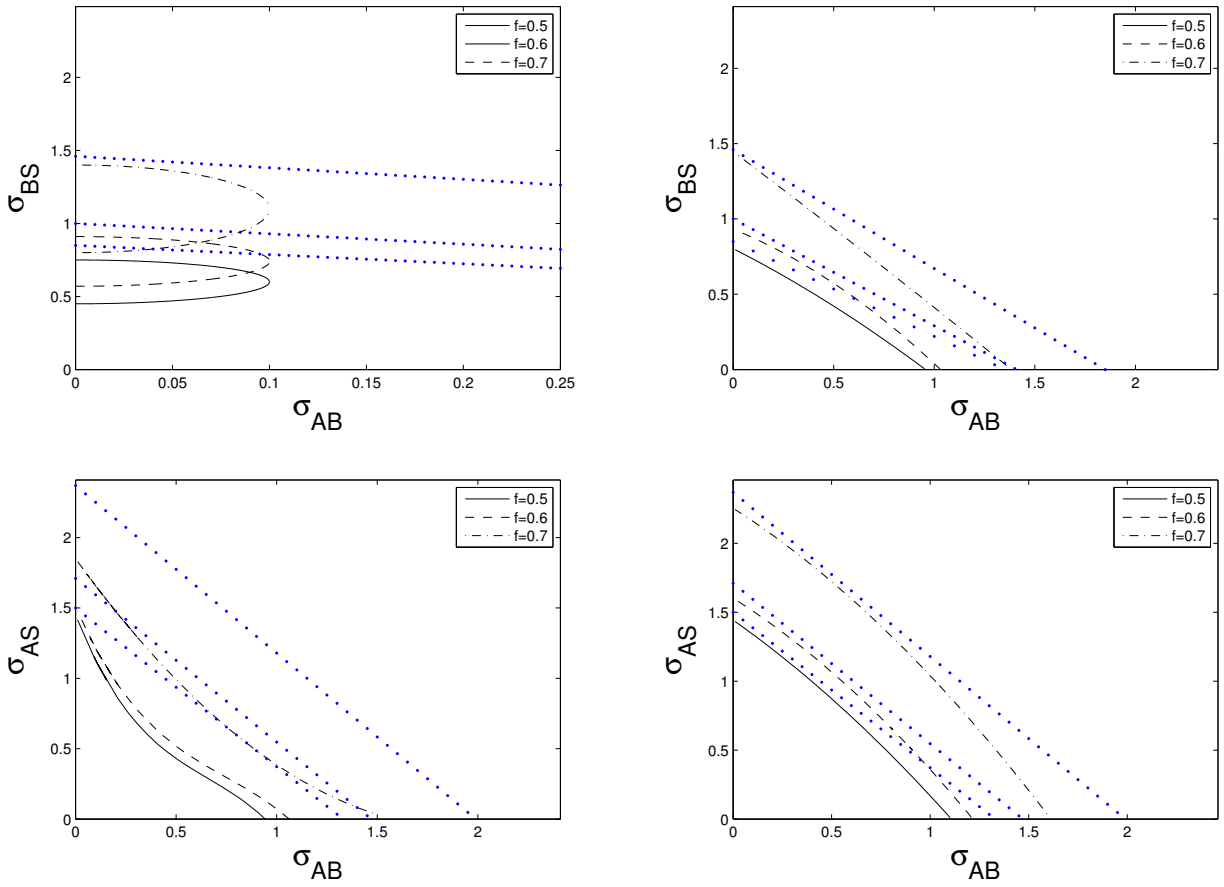

Figure 11: Three dimensional micelle neutral stability curves where $N = 2$ (top) and $N = 3$ (bottom). The figures to the left are for the small radii branch, and the figures to the right are the large radii branch of equilibria. The (blue) dotted lines represent the fold bifurcation, corresponding to $f = 0.5, 0.6, 0.7$ from bottom to top.

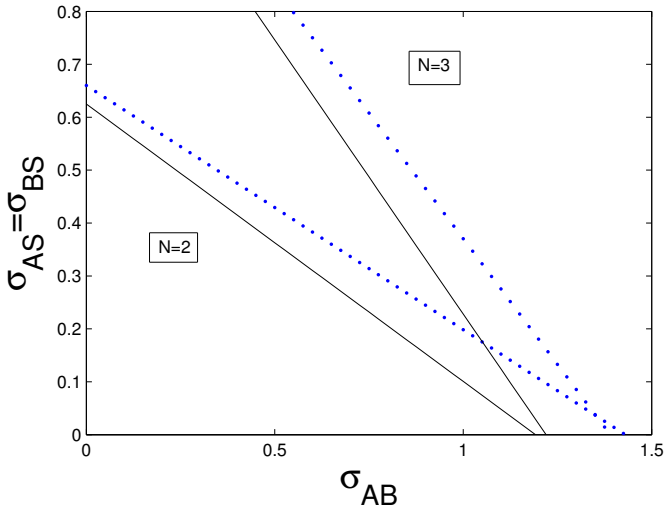

Figure 12: Vesicle neutral instability curves in terms of the interface surface energy using f=1/2 for N=2 and N=3. Unstable modes to the left of the curves and stable modes to the right of the curve. The dotted lines represent the upper existence bound on σ_{AB}, corresponding to either the infinite radius or fold bifurcations in figures 8.

4 Discussion and conclusions

In this paper, many of the basic morphologies expected in copolymer-solvent mixtures have been explored. Translational or radial symmetry allowed for detailed calculations of bifurcation and stability. Broadly speaking, there are a variety of possible stable structures, but these exist over limited parameter ranges. Instabilities give rise to many questions of dynamical development which potentially leads toward more exotic equilibria which have not been considered here.

The stability of lamellar structures runs parallel to studies of two phase copolymer mixtures [26, 27]. Placing our results back into a dimensional frame, the similarities are apparent. One common theme is that stability is moderated by competition between surface energy and the effect of polymer stretching modeled by the nonlocal term in the energy functional. The former effect resists bending of lamellar layers, whereas the latter promotes it.

Stability of two- and three layer lamellar multilayers was considered by van Gennip and Peletier [19]. They work in a variational setting, using an energy which is essentially the energy defined in (18) and (19). They find that the two-layer solution is always unstable with respect to arbitrary wavelength perturbations. At first this appears to be at odds with our findings. The difference is that [19] considers only stability of the configuration of optimal width, which they define to be the one with least energy to mass ratio. In terms of our dimensionless formulation, this would have the effect of restricting the set of parameters over which stability is computed. We have verified by numerical simulation of (4-5) that there are situations where the two layer solution is stable.

There are also connections between our results for concentric micelle-type equilibria and those for the pure diblock case studied by Ren and Wei [16]. Viewing micelle equilibria as critical points of the energy constrained by fixed polymer region volume, the resulting equilibrium free boundary problem is exactly that studied in [16]. The results in [16] indicate that the strength of the interaction parameter (here α) must be sufficiently large for existence of equilibria. Placing this in our nondimensional formulation, this means that σ_{AB} surface energy must be small, which is qualitatively consistent with our findings.

Our findings appear to translate back to the density functional model. We have checked our stability results for both lamellar and concentric states, and find they generally agree with simulations of (4-5), even in circumstances where the interface thickness is not particularly small. Instabilities appear to give rise to more exotic structures, such as those reported in numerical simulations and experiments [21, 22]. In this respect, our results should clarify the parameter regimes where radially symmetric equilibria should or should not be observed.

The study presented here dealt specifically with contiguous equilibrium structures in isolation. In greater generality, there may be competition among many of these, akin to Ostwald ripening of dilute phase separated mixtures. The interaction takes the form of mass exchange between isolated aggregates, driven by gradients of the chemical potential ν. This raises the possibility of instabilities when placed in an environment which produces an ambient chemical potential at infinity different than that imposed by the far field boundary condition (13). Here, this possibility was specifically excluded by preventing mass flux from the far field using (14).

There are many other morphological classes which have not been studied here, including double- and multiple- bubble shapes [28, 29]. In addition, there are many dynamic features left unresolved, including nonlinear effects and the evolution of weakly curved lamellar configurations (e.g. [30, 31]). The present study provides a first step to exploring the wide variety of phenomenon in copolymer-solvent systems.

Appendix: some remarks on the sharp-interface limit

Here we recall some of the standard issues needed to derive the singular limit of the equations (4-5) using matched asymptotic expansions. Much of this analysis is well documented throughout the literature [13, 14, 23], so our purpose here is to point out the unique aspects of our problem.

Away from interfaces, the quantities Φ,Ψ, μ and ν are expanded in powers of ϵ as $\Phi = \Phi_0 + \epsilon\Phi_1 + \ldots$ etc. The leading order solutions give $\Delta\mu_0 = 0 = \Delta\nu_0$, which when matched to the inner layer will give $\mu_0 = \nu_0 = 0$. This implies that $W_\Phi(\Phi_0, \Psi_0) = 0 = W_\Psi(\Phi_0, \Psi_0)$, which means that (Φ_0, Ψ_0) represents one of the three minima of W. The next order reads $\Delta\mu_1 = \alpha\Phi_0$ and $\Delta\nu_1 = 0$. After rescaling, this permits the identification of μ_1 with v and ν_1 with w in the free boundary problem.

The solution near the interfaces (inner expansion) uses a standard fitted coordinate system (ρ, s) with $\rho = \epsilon^{-1}r$, chosen so that r is the signed distance to the interface and s is the transverse coordinate (or coordinates). Expanding as before, the leading order inner problem is

$$\begin{aligned}\mu_0 &= -\Phi_{0\rho\rho} + W_\Phi(\Phi_0, \Psi_0),\\ \nu_0 &= -\Psi_{0\rho\rho} + W_\Psi(\Phi_0, \Psi_0).\end{aligned}$$

along with $\mu_{0\rho\rho} = 0 = \nu_{0\rho\rho}$. The latter implies after matching that μ_0 and ν_0 are constants, which can be shown to be zero by integration of these equations (assuming the potential W has wells of equal depth). The interface profiles represent heteroclinic orbits of this system which connect minima of W. The next order in the expansion gives a linear system

$$\begin{aligned}-\Phi_{1\rho\rho} + W_{\Phi\Phi}(\Phi^{(0)}, \Psi^{(0)})\Phi^{(1)} + W_{\Phi\Psi}(\Phi^{(0)}, \Psi^{(0)})\Psi^{(1)} &= \mu_1 + \kappa\Phi_{0\rho}\\ -\Psi_{1\rho\rho} + W_{\Psi\Phi}(\Phi^{(0)}, \Psi^{(0)})\Phi^{(1)} + W_{\Psi\Psi}(\Phi^{(0)}, \Psi^{(0)})\Psi^{(1)} &= \nu_1 + \kappa\Psi_{0\rho}\end{aligned}$$

which has a solvability condition (e.g. [23])

$$\mu_1 \left[\Phi_0\right]_-^+ + \nu_1 \left[\Psi_0\right]_-^+ = -\kappa\Sigma,$$

where the surface energy is given by the integral

$$\Sigma = \int_{-\infty}^{\infty} ({\Phi_0}_\rho^2 + {\Psi_0}_\rho^2) d\rho.$$

This quantity can also be characterized using the Γ-convergence results of Baldo [32], which does not rely on knowing the interface profiles explicitly. Expansion of the equations for μ and ν at order ϵ^2 lead to the interface velocity conditions as in the classical Cahn-Hilliard setting [13].

Because the domain under which (4-5) is considered is unbounded, this leads to a situation where the free boundary problem obtained above is potentially incompatible with the given far field boundary conditions. This can be seen directly, for example, in the one dimensional case. In the solvent region, $\mu_{xx} = 0$, which cannot be solved when imposing both a nonzero value for μ on an edge interface and $\mu(\pm\infty) = 0$.

The resolution to this apparent paradox is to introduce a "diffusion" layer into the expansion, which uses the stretched coordinate $X = \epsilon^{1/2}x$, valid where $X = O(1)$. Taking $W \approx \frac{1}{2}(\Phi^2 + \Psi^2)$ for simplicity, the equations in the new coordinates are

$$\Phi_t = \Delta\Phi - \alpha\Phi, \quad \Psi_t = \Delta\Psi, \tag{103}$$

where $\Phi = \Phi(X,t)$ and $\Psi = \Psi(X,t)$ (note ϵ has vanished entirely). These diffusion equations are supplemented with the corresponding far field boundary conditions and a boundary condition given by matching to the solution where $X = O(\epsilon^{1/2})$. Notice this means that in equilibrium for $|x| >> 1$, $\mu \sim \Phi$ solves a Helmholtz equation $\Delta\Phi = \alpha\Phi$, which admits exponentially decaying solutions as $x \to \infty$. It is therefore possible to have a nonzero interface value for μ and yet have μ decay at infinity.

Our analysis of the free boundary problem is limited to either equilibrium where $\nu \equiv \nu_\infty$, or to localized perturbations where the dynamics in the stretched region are not important. In this case, it is sufficient to impose conditions (14) which prevent the flux of either Φ or Ψ to and from infinity, which would of course be introduced by a nonzero diffusion layer.

Acknowledgment

SO was supported through a NSF-Alliance Postdoctoral award DMS-0946431. KG was supported through NSF award DMS-1514689.

[1] Karen I Winey, Edwin L Thomas, and Lewis J Fetters. Isothermal morphology diagrams for binary blends of diblock copolymer and homopolymer. *Macromolecules*, 25(10):2645–2650, 1992.

[2] Takeji Hashimoto, Satoshi Koizumi, and Hirokazu Hasegawa. Ordered structure in blends of block copolymers. 2. self-assembly for immiscible lamella-forming copolymers. *Macromolecules*, 27(6):1562–1570, 1994.

[3] Takao Ohta and Aya Ito. Dynamics of phase separation in copolymer-homopolymer mixtures. *Physical Review E*, 52(5):5250, 1995.

[4] Aya Ito. Domain patterns in copolymer-homopolymer mixtures. *Physical Review E*, 58(5):6158, 1998.

[5] T. Uneyama and M. Doi. Calculation of the micellar structure of polymer surfactant on the basis of the density functional theory. *Macromolecules*, 38(13):5817–5825, 2005.

[6] Takashi Uneyama. Density functional simulation of spontaneous formation of vesicle in block copolymer solutions. *The Journal of chemical physics*, 126(11):114902–114902, 2007.

[7] Adam Blanazs, Steven P Armes, and Anthony J Ryan. Self-assembled block copolymer aggregates: From micelles to vesicles and their biological applications. *Macromolecular rapid communications*, 30(4-5):267–277, 2009.

[8] Yiyong Mai and Adi Eisenberg. Self-assembly of block copolymers. *Chemical Society Reviews*, 41(18):5969–5985, 2012.

[9] L. Leibler. Theory of microphase separation in block copolymers. *Macromolecules*, 13:1602–1617, 1980.

[10] T. Ohta and K. Kawasaki. Equilibrium morphology of block coploymer melts. *Macromolecules*, 19:2621–2632, 1986.

[11] T. Ohta and K. Kawasaki. Comment on the free energy functional of block copolymer melts in the strong segregation limit. *Macromolecules*, 23:2413–2414, 1990.

[12] J. W. Cahn and J. E. Hilliard. Free energy of a nonuniform system I. Interfacial free energy. *J. Chem. Phys.*, 28:258–267, 1957.

[13] R. L. Pego. Front migration in the nonlinear Cahn-Hilliard equation. *Proc. R. Soc. Lond. A*, 422:261–278, 1989.

[14] Y. Nishiura and I. Ohnishi. Some mathematical aspects of the micro-phase separation of diblock copolymers. *Physica D*, 84:31–39, 1995.

[15] C. B. Muratov. Theory of domain patterns in systems with long-range interactions of Coulomb type. *Phys. Rev. E*, 66(6):066108–+, December 2002.

[16] Xiaofeng Ren and Juncheng Wei. Concentrically layered energy equilibria of the di-block copolymer problem. *European J. Appl. Math.*, 13(5):479–496, 2002.

[17] T Ohta and M Nonomura. Elastic property of bilayer membrane in copolymer-homopolymer mixtures. *The European Physical Journal B-Condensed Matter and Complex Systems*, 2(1):57–68, 1998.

[18] Yves van Gennip and Mark A. Peletier. Copolymer-homopoymer blends: global energy minimisation and global energy bounds. *Calc. Variations*, 33:75–111, 2008.

[19] Yves Van Gennip and Mark A Peletier. Stability of monolayers and bilayers in a copolymer-homopolymer blend model. *Interfaces and Free Boundaries*, 11:331–373, 2009.

[20] Karl Glasner. Multilayered equilibria in a density functional model of copolymer-solvent mixtures. *SIAM Journal on Mathematical Analysis*, 49(2):1593–1620, 2017.

[21] Edgar Avalos, Takeshi Higuchi, Takashi Teramoto, Hiroshi Yabu, and Yasumasa Nishiura. Frustrated phases under three-dimensional confinement simulated by a set of coupled cahn–hilliard equations. *Soft matter*, 12(27):5905–5914, 2016.

[22] Hiroshi Jinnai, Richard J Spontak, and Toshio Nishi. Transmission electron microtomography and polymer nanostructures. *Macromolecules*, 43(4):1675–1688, 2010.

[23] Lia Bronsard, Harald Garcke, and Barbara Stoth. A multi-phase mullins–sekerka system: Matched asymptotic expansions and an implicit time discretisation for the geometric evolution problem. *Proceedings of the Royal Society of Edinburgh: Section A Mathematics*, 128(03):481–506, 1998.

[24] Xiaofeng Ren and Juncheng Wei. On the multiplicity of solutions of two nonlocal variational problems. *SIAM Journal on Mathematical Analysis*, 31(4):909–924, 2000.

[25] Karl Glasner and Saulo Orizaga. Improving the accuracy of convexity splitting methods for gradient flow equations. *Journal of Computational Physics*, 315:52–64, 2016.

[26] Xiaofeng Ren and Juncheng Wei. On the spectra of three-dimensional lamellar solutions of the diblock copolymer problem. *SIAM journal on mathematical analysis*, 35(1):1–32, 2003.

[27] Saulo Orizaga and Karl Glasner. Instability and reorientation of block copolymer microstructure by imposed electric fields. *Physical Review E*, 93(5):052504, 2016.

[28] T Ohta and M Nonomura. Formation of micelles and vesicles in copolymer-homopolymer mixtures. *Formation and Dynamics of Self-Organized Structures in Surfactants and Polymer Solutions*, pages 127–130, 1997.

[29] Xiaofeng Ren and Juncheng Wei. A double bubble in a ternary system with inhibitory long range interaction. *Archive for Rational Mechanics and Analysis*, pages 1–53, 2013.

[30] Karl B Glasner and Alan E Lindsay. The stability and evolution of curved domains arising from one-dimensional localized patterns. *SIAM Journal on Applied Dynamical Systems*, 12(2):650–673, 2013.

[31] Shibin Dai and Keith Promislow. Geometric evolution of bilayers under the functionalized cahn–hilliard equation. *Proceedings of the Royal Society A: Mathematical, Physical and Engineering Science*, 469(2153), 2013.

[32] Sisto Baldo. Minimal interface criterion for phase transitions in mixtures of cahn-hilliard fluids. In *Annales de l'IHP Analyse non linéaire*, volume 7, pages 67–90, 1990.